

Location-Aware Self-Supervised Transformers

Mathilde Caron Neil Houlsby Cordelia Schmid
Google Research

Abstract

*Pixel-level labels are particularly expensive to acquire. Hence, pretraining is a critical step to improve models on a task like semantic segmentation. However, prominent algorithms for pretraining neural networks use image-level objectives, e.g. image classification, image-text alignment à la CLIP, or self-supervised contrastive learning. These objectives do not model spatial information, which might be sub-optimal when finetuning on downstream tasks with spatial reasoning. In this work, we propose to pretrain networks for semantic segmentation by predicting the relative location of image parts. We formulate this task as a classification problem where each patch in a query view has to predict its position relatively to another reference view. We control the difficulty of the task by masking a subset of the reference patch features visible to those of the query. Our experiments show that this **location-aware** (LOCA) self-supervised pretraining leads to representations that transfer competitively to several challenging semantic segmentation benchmarks.*

1. Introduction

Spatial annotations are extremely time consuming and costly to acquire. Therefore, pretraining is commonly used to improve performance and label-efficiency of models reasoning at the pixel-level, such as semantic segmentation models. The dominant method for pretraining neural networks uses image-level tasks on massive amounts of supervised data [12, 49, 51, 70, 72]. For example, powerful foundation models such as the recent Flamingo [1], CoCa [69] or PaLI [14] models, build upon a visual encoder pretrained by matching aligned image and text pairs with a contrastive loss [49], or by classifying images into a predefined set of categories [72]. These two standard supervised pretraining objectives operate at the global (whole image) level, without explicitly encouraging spatial reasoning.

However, it is unclear whether image-level pretraining is the optimal strategy when targeting recognition tasks with

spatial understanding. In fact, a recent study by Minderer *et al.* [43] shows that some models pretrained with image classification, while being excellent at image-level downstream tasks, transfer poorly to object detection, a task clearly requiring spatial reasoning. Motivated by their observation, our goal is to design a pretraining strategy leading to strong features for pixel-level downstream tasks. Specifically, we target semantic segmentation in this work.

We argue that the main reason why pretraining is usually done with global objectives is because annotations are much easier to collect at the image level rather than at the pixel level. Indeed, the image classification or image-text datasets typically used in state-of-the-art systems [49, 72] are orders of magnitude bigger and cover more categories than densely annotated datasets [39, 73]. Therefore, one approach to unlock the potential of dense, spatially-aware pretraining at scale might be to move away from annotations, as proposed by self-supervised learning (SSL) approaches. A successful branch of SSL, often coined as “contrastive learning”, works by matching the representation of different views obtained from a same image by means of data augmentation [10, 13, 29, 32]. Interestingly, Caron *et al.* [11] have shown that segmentation masks emerge from the attention maps of Vision Transformers (ViT) [23] trained with these contrastive methods. However, we found in our preliminary experiments that salient attention maps do not correlate with superior performance after finetuning to the semantic segmentation task [76]. We hypothesize that this is because contrastive methods operate at the global level without explicitly encouraging spatial relationships. Worse, due to their intensive use of spatial data augmentation such as cropping and rescaling, they tend to produce localization-invariant features discarding spatial information [3, 16]. Successful alternative strategies to contrastive methods have recently emerged [5, 6, 31, 64, 68, 71]. Of particular interest, masked autoencoders propose to reconstruct masked content [6, 31], hence encouraging Transformers to learn about relationships between different image parts.

In this paper, we explore an alternative to content reconstruction to encourage the emergence of spatial Transformer features, that of predicting relative image parts location. Specifically, our **location-aware** approach, LOCA, simply

Correspondence: mcaron@google.com. Code will be released at: <https://github.com/google-research/scenic/tree/main/scenic/projects/loca>

works by predicting the location of a *query* view relatively to another, *reference*, view as illustrated in Fig. 1. In order to solve the relative position task, the Transformer needs to reason about the spatial and semantic relationships between different parts of an image. In practice, this pretext task admits a simple formulation: we implement our model as a classification problem where each patch in the query view is trained to predict its position relatively to the reference view. To be able to locate themselves in the reference, the query patch features “look” at the reference through a shallow cross-attention module. We show that we can control the difficulty of the task and properties of the resulting features by masking reference patch features to the query. We add a patch feature prediction objective to our localization framework, explicitly encouraging patches covering similar locations to have consistent representations. Overall, our location-aware pretraining can be seen as revisiting the pioneering SSL works on “Context prediction” [22, 46] in the context of Vision Transformers, which has attracted only very limited attention so far [17, 71].

Our experiments show that LOCA yields excellent locality and good semantic understanding, while still being a little behind state-of-the-art methods on the pure semantic understanding axis. Overall, this yields improved performance over state-of-the-art supervised [55, 59] and unsupervised [11, 15, 31, 74] representation learning methods for Vision Transformers when transferred to semantic segmentation, which requires both local and semantic features. Finally, we also show that our method scales promisingly to large models and large amount of data, which is a positive signal that LOCA could be a viable candidate for spatially-aware pretraining at scale.

2. Related Work

SSL with location prediction. Pioneering works in SSL proposed to exploit spatial cues to generate pretext tasks [22, 28, 35, 37, 45, 46, 52]. Notably, inspired by word2vec [42], Doersch *et al.* [22] train a network to predict the relative position of a pair of patches from the same image while Noroozi and Favaro [46] extend this approach to solving “jigsaw puzzles” by rearranging a set of shuffled crops of an image. These approaches were developed with Convnets and very little work has revisited them in the scope of Transformers [71]. Zhai *et al.* [71] propose to pre-train a ViT to predict the position of its input patches given their visual appearance only, i.e. by discarding positional embeddings. We compare this strategy to the LOCA mechanism in Fig. 2 and Sec. 4.1. Also using localization, UP-DETR [20] propose to pretrain the DETR [8] architecture without using any annotations by localizing random boxes in a reference image. Our initial design is inspired by UP-DETR, though our implementations vary greatly: we formulate our task as a patch position classification problem

while they follow DETR losses and architecture.

Context and masked auto-encoders. Also exploiting spatial cues for SSL, Pathak *et al.* [47] propose context auto-encoders to train Convnets to generate the content of a masked region based on its surrounding. Recently, masked auto-encoders revisit this “inpainting” approach to pretraining Vision Transformers [6, 31, 62]. Specifically, the task is to reconstruct masked [6] or dropped [31] patches from the input sequence tokens, either directly in pixel space [31] or in feature space [6, 62, 74]. Similar to our approach, masked auto-encoders are trained with patch-based objectives with a task encouraging the network to learn local representations of object parts and their spacial arrangement.

Dense contrastive SSL. A prominent line of SSL, often referred to as “contrastive” or “siamese” approaches, trains networks by matching the representation of different views obtained from a same image by means of data augmentation [3, 10, 13, 24, 29, 32, 65]. These approaches have primarily been developed with global (image-level) objectives but several recent works have adapted them to learn local features [48, 50, 61, 66, 67]. Specifically, instead of matching representations from global descriptors, they match features that come from the same location in the original image but seen from different views [48]. Our feature prediction loss is directly inspired from this literature. Also, we borrow the strategy of back-tracking the data augmentation process of two views to find their regions that intersect [48].

Unsupervised semantic segmentation. While our goal is to improve pretraining for semantic segmentation, some works directly target semantic segmentation without using any supervision at all [18, 60]. Indeed, Caron *et al.* [11] have shown that unsupervised segmentation masks emerge from the attention module of ViTs trained with image-level contrastive objectives such as DINO. Several works build on this observation and enhance self-supervised features to produce completely unsupervised segmentation masks [30, 54, 76]. These approaches typically do not evaluate semantic segmentation after end-to-end finetuning.

3. Methodology

3.1. Query-reference mechanism

In our work, we propose a query-reference mechanism to predict image parts localization. Specifically, a query has to predict its position as viewed in a reference image as illustrated in Fig. 1. We consider a single query per reference in this section for simplicity but use several in practice. We now detail our query-reference mechanism.

Generating query and reference views. From an image x of a dataset, we form a *reference* view (denoted by

x_{ref}) and a *query* view (denoted by x_q) using a randomized data augmentation routine composed of flipping, cropping, rescaling and color jittering. Because query and reference are generated by two independent augmentation draws, they usually have different image statistics (i.e. different scale, region or color histogram). This forces the network to rely less on low-level cues (chromatic aberration, color, and edge consistency) to solve the localization task and more on recognizing object parts and their organization.

The query’s task is to locate itself inside the reference view and therefore our loss is defined only at the intersection of the two views. Hence, we wish the query and reference to intersect often. Also, in order to favor the emergence of image-*part* representations, we constrain the spatial extent of the queries. A natural choice then is to sample the reference view so that it covers a large area of the original image and the query views so that they cover a small portion of the original image. In practice we use the MSN input pipeline [3] with random resize-cropping and patch-dropping for generating 10 different query views per reference. Note that as opposed to MSN, our goal is not to have an identical representation for the different generated views but to predict their positions relatively to a reference view.

Correspondences between query and reference. Following the standard protocol of the Vision Transformers [23], query and reference views are divided into non overlapping patches of resolution $P \times P$. More precisely, the reference view is flattened into $N_{ref} = \lfloor H_{ref}/P \rfloor \times \lfloor W_{ref}/P \rfloor$ (with $H_{ref} \times W_{ref}$ the resolution of x_{ref}) separate patches $x_{ref}^i, i \in \{1, \dots, N_{ref}\}$. Default typical values are $H_{ref} = W_{ref} = 224, P = 16$ and $N_{ref} = 196$. A similar “patchification” process is applied on the query view, resulting in a sequence of N_q patches $x_q^j, j \in \{1, \dots, N_q\}$. Unless specified otherwise, we have $N_q = 36$. By backtracking the data augmentation draws that generated x_{ref} and x_q , we can identify the patch-level correspondences between these two views. In particular, we know a function h that, given any patch position j in the query view, returns the position $i = h(j)$ of the patch in the reference, $x_{ref}^{h(j)}$, that has the greatest overlap with the query patch x_q^j . We implement the function h with successive nearest interpolations and because the patchification grids of x_q and x_{ref} are usually not exactly aligned, a pair of matching patches, x_q^j and $x_{ref}^{h(j)}$, have similar content but do not generally match perfectly. This effect can be seen in the example in Fig. 1.

3.2. Relative localization training

We process both the reference and query views with a Vision Transformer network [23], denoted by f , of internal dimension d : $d = 768$ for ViT-B and $d = 1024$ for ViT-L. We note $Z_q \in \mathbb{R}^{d \times N_q}$ (resp. $Z_{ref} \in \mathbb{R}^{d \times N_{ref}}$), the output patch representation matrix of the query (resp. reference)

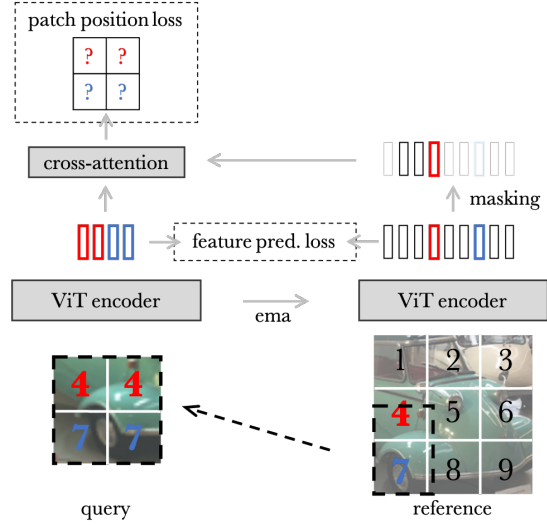


Figure 1. **LOCA** works by predicting the location of a query view relatively to a reference view. Patch features of the query look at those of the reference through a cross-attention block before making their prediction. We control the difficulty of the task by masking part of the reference patch features visible to the query. We also use a feature prediction loss to encourage patches covering similar content in different views to be consistent.

view. In the following, we detail the self-supervised localization loss applied to these patch representations.

Patch position prediction. We implement the query localization problem as a N_{ref} -way classification task where each query patch representations has to predict the position of the patch covering the same content in the reference view, as given by h . To that end, the patch representations of the query need to be able to “look” at those of the reference. We implement this query-reference interaction with a single cross-attention transformer block, denoted by g , whose queries are computed from Z_q and keys and values are obtained from Z_{ref} . We denote the query representations after they have looked at the reference as $G = g(Z_q, Z_{ref}) \in \mathbb{R}^{d \times N_q}$ and by $W \in \mathbb{R}^{d \times N_{ref}}$ the final “position classification” layer. Note that N_{ref} is the total number of positions in the reference. We train the network to minimize the following position prediction loss:

$$\frac{1}{|\Omega|} \sum_{j \in \Omega} \ell((W^T G)_j, h(j)) \quad (1)$$

where Ω is the set of patch position in the query that has an intersection with the reference (i.e. where h is defined) and ℓ is the standard softmax cross-entropy loss. We average the loss over both the different query views and the minibatch, and learn f, g , and W parameters with back-propagation.

Masking reference patch features visible to the query.

In practice, we find that problem 1 can be solved near per-

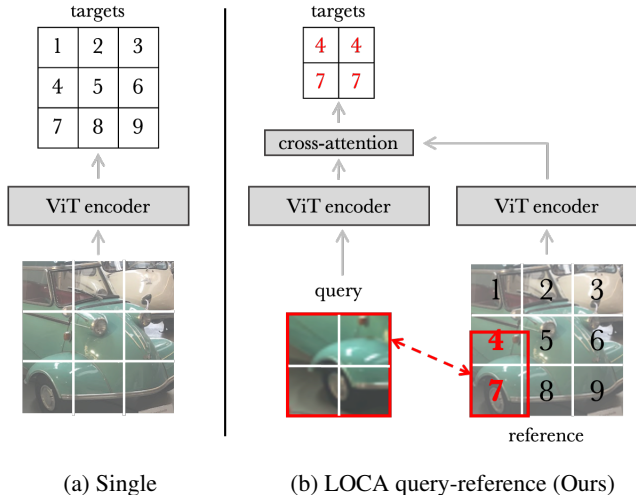


Figure 2. **Conceptual comparison of single vs query-reference** patch position prediction mechanisms: (a) in a single view as in Zhai *et al.* [71]; (b) in a query view relatively to a reference view as in LOCA (Ours). Quantitative comparison is presented in Fig. 3. Masking is not illustrated here for simplicity.

factly by the network (see the validation accuracy in Fig. 3). As empirically shown in Sec. 4.1, one strategy to make the task more challenging is to restrict what the query can see from the reference. We implement this mechanism by randomly dropping (or “masking”) a ratio η of the patch features input to the cross-attention block g . Specifically, we redefine $G = g(Z_q, m(Z_{ref}, \eta))$ where m is a random process that discards $\lfloor \eta N_{ref} \rfloor$ columns of Z_{ref} . We use structured dropping (i.e. we keep a consecutive subset of patch tokens) as we find in our experiments that it leads to superior performance than unstructured dropping (+0.8 mIoU).

Patch feature prediction. Inspired by UP-DETR framework [20], we add a patch feature prediction objective to our localization framework in order to obtain more semantic representations. Intuitively, the patch features should not only be able to locate themselves but also to match those at a similar location in a different context. We implement this with a patch-based version of the MSN framework [3] (see Appendix A). Specifically, we use Sinkhorn-Knopp [2, 10] and me-max regularization [4] schemes to prevent the collapse of the representations, as well as an exponential moving average (ema) branch [32] for the encoder processing the reference view. We use the default values from MSN [3] for the temperature, momentum and me-max parameters. Other patch feature prediction implementations are possible [11, 13, 32]. We have observed in our preliminary experiments that this choice has minimal impact on the final performance and we choose MSN for its stability. Overall, we show in Table 5 that adding the patch feature prediction loss brings a substantial boost of performance in our model.

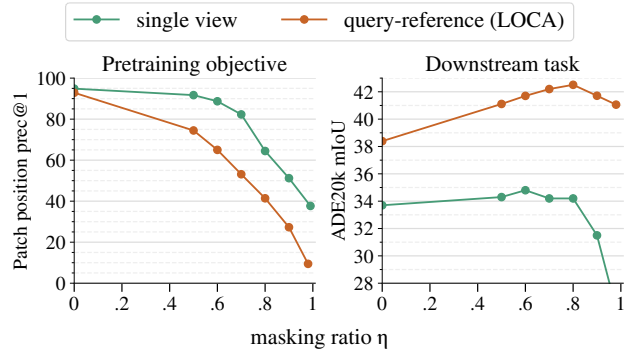


Figure 3. **Single vs query-reference** patch position prediction mechanisms. For both mechanisms, we report the position prediction accuracy (left) and the performance after transfer to semantic segmentation on ADE20k (right) for different patch masking ratios η . Query-reference makes for a more challenging pre-training objective (lower accuracy on the position prediction task) due to different image statistics between query and reference and constrained patch interactions. Conceptual differences are illustrated in Fig. 2. Varying the masking ratio controls the difficulty of the task and improves transfer performance.

3.3. Implementation and evaluation protocol

Implementation details. We train our models with a learning rate of 0.001 (decayed with cosine schedule), a batch size of 1024 and a fixed weight decay of 0.1 with adamw optimizer [41]. We use ImageNet-1k or ImageNet-21k without labels as our pre-training dataset [51]. Models for ablations and analyses (in Sec. 4.1 and 4.3) are trained during 100 epochs while those in Sec. 4.2 and 4.4 are trained for 600 epochs. 100 epochs of training on 16 TPUv2 accelerators take 29 hours. We use $\eta = 0.8$ for masking (see effect in Fig. 4), resulting in 40 keys and values in input of the cross-attention block. Additional implementation details are in the Appendix A. We implement LOCA in Jax. Code and models to reproduce our results will be made publicly available as a SCENIC project [21].

Evaluation protocol on semantic segmentation. We evaluate our models by end-to-end finetuning on the following 4 semantic segmentation benchmarks: ADE20K [73], Pascal Context [44], Pascal VOC [25] and Cityscapes [19]. Recent works have shown that plain ViT architectures can be used for dense recognition tasks [38, 43, 56]. Therefore, we follow the linear decoder protocol of Strudel *et al.* [56] hence using a minimal amount of adapter layers to prevent the effect of pretraining of being washed out by heavy decoders. We validate in Appendix B that we reproduce the implementation of Strudel *et al.* [56]. We report results in single scale mode, averaged over 5 runs as we typically observe a standard deviation of ± 0.4 mIoU on ADE20k. All evaluation implementation details are in Appendix B.

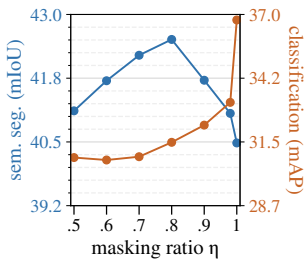


Figure 4. **Masking reference patches to the query** improves both classification and segmentation transfers on ADE20k. However, too extreme masking prevents the query from solving the task by relative localization which hurts localization transfer. See second § of Sec. 4.1.

4. Experiments

4.1. Our Localization Mechanism

In this section, we detail our design choices for the localization task: we study the query-reference mechanism, analyze and visualize the effect of masking reference patches and evaluate different loss functions. Models are run without the feature prediction framework (i.e. with loss (1) only) to better understand the effect of pure localization training.

Query-reference mechanism. We compare the two mechanisms illustrated in Fig. 2. Note that removing positional embeddings in the “single” strategy is crucial, otherwise the task is trivial [71]. To avoid confounding factors, we also discard positional embeddings in the query view in LOCA in this experiment, though we find in practice it has minor effect on the performance (see Tab. 5). For both strategies, we vary η , the proportion of masked patch tokens. In “single” mechanism, masking patch tokens means that the patches can only attend to the unmasked patch tokens, i.e. only the unmasked patches take part in the computation of keys and values of ViT [71]. We run a small hyper-parameter grid for all runs. The results are in Fig. 3. On the left panel, we report the validation accuracy for the position prediction task after 100 epochs of training. This measures how well the network solves its pretraining objective in a fixed training budget, which enables the comparison of the difficulty of different pretraining strategies. On the right panel, we show the models transfer performance.

Table 1. **Localization loss.** We evaluate several variants for the query localization loss and report mIoU on ADE20k semantic segmentation transfer. Predicting the position of all patches versus the position of the central patch only is better, likely because it involves reasoning about the spatial extent of the query. Classification works better than regression in our experiment, despite the fact that regression is advantageously not impacted by the misalignment between query and reference patchification grids.

Output	Predicts spatial extent	Loss	ADE20k
Every patch position	✓	Classif.	42.5
Central patch position		Classif.	38.6
Query box coordinates	✓	Regress.	39.0

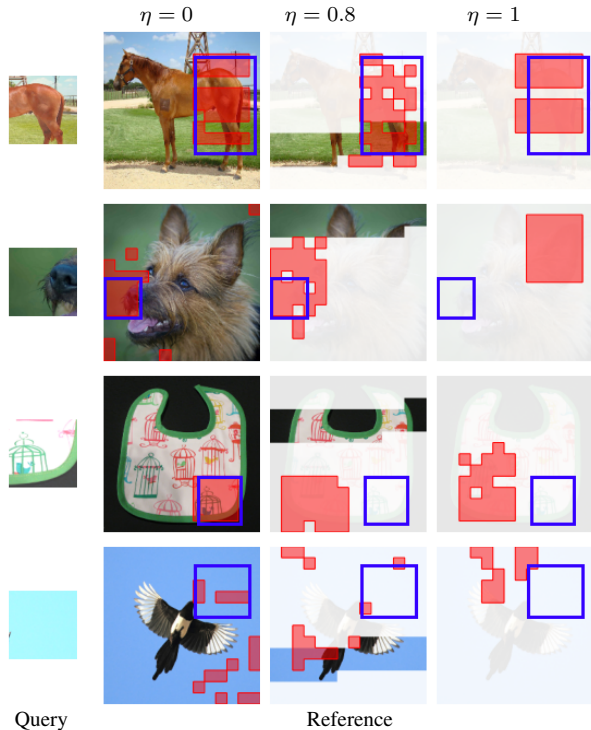


Figure 5. **Visualizing LOCA’s predictions.** The query location is shown in blue in the reference and LOCA predictions are shown in red. Columns correspond to different reference η masking rates and we show only patches visible to the query when it makes its prediction. More examples in the Appendix D. Displayed images are not seen during training. See discussion in third § of Sec. 4.1.

We see in Fig. 3 that the query-reference mechanism of LOCA is a more challenging pretraining task than predicting position in a single view as in Zhai *et al.* [71] and leads to better representations for semantic segmentation. This can intuitively be explained by several conceptual differences. First, in the single mechanism, the network can almost perfectly solve the task by leveraging low-level non-semantic cues such as chromatic aberration, color or edges consistency between patches. This is *partly* prevented in the query-reference mechanism due to different image statistics between query and reference (thanks to cropping, rescaling and color jittering). Second, the way query (i.e. patches that predict a position) and reference (i.e. context patches) can interact is in stark contrast in the two mechanisms. In “single”, query and reference are the same and hence interact in an unconstrained manner at all stages of the computation. With masking, Zhai *et al.* [71] modify partly this design by now processing each query patch independently but still allowing them to fully attend to the reference patches at each block. By contrast, in LOCA, query patches can attend freely to each other but cannot look at the reference patches until the last stage of the network. Intuitively, this more constrained interaction encourages both query and reference patches to develop stronger final localization features.

Table 2. **Comparison with previous results on semantic segmentation.** We report mean IoU for semantic segmentation on the validation set of ADE20k [73], Cityscapes [19] and Pascal Context (“P.Context”) [44] for different self-supervised and supervised pretraining methods. We consider two settings: (i) pretraining on ImageNet-1k with ViT-Base and (ii) pretraining on ImageNet-21k with ViT-Large. Networks are then end-to-end finetuned on the semantic segmentation train set. We follow the experimental setup of Segmenter [56] for end-to-end finetuning of ViT with linear decoder. We report their number for the supervised checkpoints “DeiT” and “Augreg”. Results for the self-supervised methods and for DeiT-III are run by us from official released checkpoints. We report the average over 5 runs with single-scale mode (*: numbers with multi-scale evaluation).

Method	Supervised	ADE20k	P.Context	Cityscapes
<i>ImageNet-1k / ViT-Base</i>				
Random init.		21.1	19.6	51.4
DINO [11]		44.1	50.7	78.4
MoCo-v3 [15]		45.4	51.6	78.6
MAE [31]		45.5	51.7	79.7
DeiT [56,58]	✓	47.1	–	–
DeiT-III [59]	✓	47.3	53.9	79.7
iBOT [74]		47.0	54.6	79.8
LOCA (Ours)		47.9	54.9	79.8
<i>ImageNet-21k / ViT-Large</i>				
Augreg [55,56]	✓	50.7	56.5*	80.7*
LOCA (Ours)		52.3	60.3	81.5

Masking reference patches. In Fig. 3, we observed that the localization pretraining task can be solved near perfectly when all the patches in the reference are visible to the query (see left panel of Fig. 3 for $\eta = 0$). Restricting patches visible to the query makes the pretraining objective more challenging and leads to better representations. In Fig. 4, we analyze this effect further. We consider different masking ratios and report for the same downstream dataset both the transfer performance on semantic segmentation and multi-label classification (with frozen backbone) by turning the semantic segmentation annotations into classification labels. We observe in Fig. 4 that masking improves both localization and classification capabilities of the network. Intuitively this is because masking reference patches forces the query to rely less on finding matching salient points between the two views and more on recognizing object categories and their parts.

However, when masking becomes too aggressive, the query does not see enough of the reference to solve its task by relative localization and resorts to other cues. To understand this phenomenon, we push masking to extreme rates and even report performance when the reference is *not visible at all* ($\eta = 1$). Surprisingly, we find that the query still manages to solve the localization pretraining task to some extent with a localization accuracy of 3.7% while random

Table 3. **Fewshot semantic segmentation on ADE20k.** We report mean IoU for semantic segmentation on the validation set of ADE20k for different pretrained models. Only a fraction (either 1/32, 1/16, 1/8, 1/4 or 1/2) of ADE20k training images are used for finetuning. Results are averaged over 5 different splits. Architecture is ViT-B for all runs and pretraining data is ImageNet-1k.

Method	1/32	1/16	1/8	1/4	1/2
DINO [11]	18.4	24.5	29.5	35.2	39.5
MoCo-v3 [15]	17.7	25.2	30.8	36.5	40.7
MAE [31]	18.4	25.3	30.5	36.1	40.6
Supervised - DeiT-III [59]	20.9	27.1	32.7	38.3	42.0
iBOT [74]	20.9	28.0	33.4	38.7	42.6
LOCA (Ours)	22.2	30.0	34.4	39.1	42.8

guessing would achieve 0.5%. We hypothesize that two ways of solving the task without looking at the reference are to (i) learn where things are typically located in images and (ii) memorize all the dataset images. We argue that the “memorization” regime is akin to an implicit formulation of the “exemplar” instance discrimination approach of Dosovitskiy *et al.* [24] where the network learns to recognize each individual instance of a dataset (but without a classifier of the size of the dataset as in [24]). Overall, both learning biases of general dataset statistics and instance discrimination have been shown to improve transfer performance on classification downstream tasks [24,26,65] which is consistent with the boost in classification observed for $\eta = 1$.

Finally, this experiment shows that an optimal masking ratio for semantic segmentation features is high, but not too high either so that the network can still solve the task by *relative localization*. In practice, we use $\eta = 0.8$.

Visualizing LOCA’s predictions. In Fig. 5, we visualize the output of location prediction models trained with different masking rates: $\eta = 0$ (no masking), $\eta = 0.8$ (default) and $\eta = 1$ (invisible reference). The first row shows a situation where the network can make a valid guess about the query’s location solely based on the query visual appearance, i.e. without looking at the reference. In the second row, we see that LOCA successfully locates the snout of the dog based on the reference ear patches. This suggests that it has learned about spatial arrangement of different parts of a dog. Third row depicts the case where the network can leverage low-level cues such as edge consistency to locate the query. The masked variants are restrained in their use of such cues and hence fail to locate the query. Finally, in last row, there is no visible cue in the query that allows its localization. The prediction is degenerated for all the variants.

Choice of localization loss. In Fig. 1, we evaluate different losses for position prediction. First, we compare predicting the position of all patches versus the position of the

Table 4. **Disentangling localization and classification on semantic segmentation.** We report classification only (with a multi-label classification training) and localization only (with an oracle giving the class of the segmentation masks) evaluations on 4 popular semantic segmentation benchmarks: ADE20k [73], Pascal Context (“P.Cont.”) [44], Pascal VOC (“P.VOC”) [25] and Cityscapes (“City.”) [19]. Details about the classification/location only protocols are in Sec. 4.2. Best number is in bold and second best is underlined. We report performance for different methods pretrained on ImageNet-1k (with or without labels) with ViT-B. LOCA yields excellent locality and good semantic understanding but is still behind image-level pretraining methods on the pure semantic axis (classification only evaluation).

Method	Classification only (mAP)				Localization only (mIoU)				Both (mIoU)			
	ADE20k	P. Cont.	P. VOC	Citysc.	ADE20k	P. Cont.	P. VOC	Citysc.	ADE20k	P. Cont.	P. VOC	Citysc.
<i>Image-level pretrainings</i>												
DINO [11]	61.6	67.7	89.9	81.5	64.5	71.6	78.7	79.6	44.1	50.7	74.7	78.4
MoCo-v3 [15]	61.1	69.3	93.6	82.1	66.2	73.7	79.0	79.9	45.4	51.6	74.3	78.6
Supervised (DeiT-III [59])	64.8	71.5	94.6	<u>84.0</u>	66.5	73.6	<u>80.1</u>	80.7	<u>47.3</u>	<u>53.9</u>	<u>76.3</u>	<u>79.7</u>
<i>Spatially-aware pretrainings</i>												
MAE [31]	59.0	67.6	92.8	84.3	<u>67.0</u>	<u>74.3</u>	79.9	<u>81.1</u>	45.5	51.7	75.4	<u>79.7</u>
LOCA (Ours)	<u>62.2</u>	<u>69.9</u>	<u>93.7</u>	83.6	67.9	75.4	80.5	81.4	47.9	54.9	76.6	79.8

central patch only. We see in Fig. 1 that all patches is better. We hypothesize that this is because it requires to predict the spatial extent of the query and not just an anchor point. Second, we compare solving a per-patch position classification problem versus regressing the coordinates of the query box in the reference. For box prediction, we use a linear combination of ℓ_1 loss and the generalized IoU loss, following UP-DETR [8, 20]. Because query and reference patchification grids are usually not aligned, matching patches in query and reference do not have exactly the same content. This does not affect the box regression formulation, which might give it an advantage over per-patch classification. However, we surprisingly find in Fig. 1 that box regression leads to poorer performance than per-patch classification. It is possible that this loss requires additional hyper-parameter tuning (we performed a small optimization hyperparameter search but did not vary from the loss parameters from [8, 20]).

Overall, patch position classification is a simple implementation of our relative localization problem and works well in practice. It is possible that refinements (for example in the spirit of ROIAlign for detection [33]) lead to superior performance in the future.

4.2. Comparison with previous results

Self-supervised features have been shown to outperform supervised representations in many papers [10, 11, 29, 31]. However, as the self-supervised field makes important progress, supervised training recipes also improve greatly [40, 53, 55, 58, 59]. In this section, we try to keep the comparison up-to-date by considering state-of-the-art ImageNet supervised ViTs, namely AugReg [55] on ImageNet-21k and DeiT-III [58] for ImageNet-1k only. We also compare to popular state-of-the-art SSL models for ViTs: DINO [11], MoCo-v3 [15], MAE [31] and iBOT [74].

Comparison on semantic segmentation benchmarks.

In Tab. 6, we report the performance of different pretraining strategies after end-to-end finetuning on semantic segmentation on the popular ADE20k, Pascal Context and Cityscapes benchmarks [19, 44, 73]. We use the linear decoder from Segmenter [56] as detailed in Sec. 3.3 and Appendix B. Results in Tab. 6 validate that representations learned with LOCA transfer well to semantic segmentation. Our performance improves over previous self-supervised and supervised representation learning methods by a margin of 0.6–1.8. Notably, we outperform the strong Augreg supervised checkpoint that was finetuned on high resolution images (384×384). We further analyze semantic segmentation performance in the following paragraph by disentangling the classification and localization aspects.

Localization and classification trade-off. Semantic segmentation is the coupling of classification and localization, where these two tasks can have different feature preferences. In Tab. 4, we propose to disentangle classification and localization performance on semantic segmentation benchmarks which require both. First, we discard local information and evaluate classification only by finetuning with a multi-label binary cross-entropy loss. Second, we evaluate localization only by reporting the performance of an already finetuned semantic segmentation model in presence of a class oracle. Specifically, the oracle replaces the label of each mask by the label of the ground truth mask it has the best IoU with. This evaluation allows to assess the shape and localization of the predictions but not their class.

In Tab. 4, we compare the behavior of models pretrained with an image-level versus spatially-aware objective only. We observe that models pretrained with a global, image-level objective such as DeiT-III or MoCo-v3 tend to be better on the classification aspect. By contrast, models trained with a spatially-aware objective such as MAE or

Table 5. **Ablation study.** We ablate different component of LOCA, one at a time. All variants are run during 100 epochs and we report their absolute and relative (Δ) performance (mIoU) after finetuning on semantic segmentation.

Variant	ADE20k	Δ
LOCA	46.2	
1 w/o positional embeddings	45.9	- 0.3
2 w/ 5 queries instead of 10	45.5	- 0.7
3 w/o color data augmentation	44.6	- 1.6
4 w/ 2 queries instead of 10	43.4	- 2.8
5 w/o feature prediction loss	42.5	- 3.7

LOCA produce more spatially accurate predictions. Overall, LOCA yields excellent locality and good class-level understanding (while not beating representations learned with label classification pretraining [59] on the pure classification axis). This results in strong semantic segmentations which require both locality and semantic features.

Label-efficient semantic segmentation. In Tab. 3, we propose to evaluate transformer features when finetuning on semantic segmentation with access to only a small amount of annotations. In particular, following Hu *et al.* [34], we randomly sample 1/2, 1/4, 1/8, 1/16 and 1/32 training images from ADE20k and use only those images to finetune our model. In the 1/32 split, as few as 630 images from ADE20k training set are used. We report the average over 5 different folds [34]. The results are in Table 3. We observe that our spatially-aware pretraining improves label-efficiency of semantic segmentation models. Interestingly, the gap with previous works become larger when very few images are available for finetuning.

4.3. Ablation Study

Table 5 shows an ablation study of several components of our model. The design choices regarding the relative localization objective have been discussed in details in Sec. 4.1. In Tab. 5, we see that adding the feature prediction loss brings a boost of +3.7 (row 5). Besides, reducing the number of queries per reference, for example 5 instead of 10, allows to speed up pretraining time by $\times 1.6$ while inducing a loss of only 0.7% in performance (see rows 4 and 2). Finally, we observe that our model is quite robust to the ablation of position embeddings (row 1) or color jittering augmentation (row 3).

4.4. Preliminary scaling behavior

A premise of SSL is that it can in theory scale to arbitrary large datasets since images don't require any annotations. In this work, we have demonstrated the potential of location-aware pretraining for a task such as semantic segmentation.

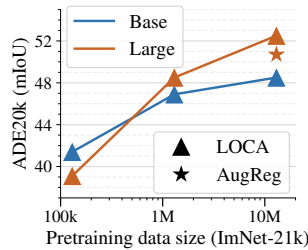


Figure 6. **Scaling study.** We report transfer performance on ADE20k for different pre-trained models. X-axis shows the size of the subset of ImageNet-21k used for pre-training. Scaling both dataset size and model capacity results in the best of transfer performance.

Since location-aware *supervised* pretraining is not feasible in practice due to the huge cost of pixel-level annotations, we believe our self-supervised spatial pretraining could be a good candidate for scaling. Our hope is that scaling both dataset and model axes improves the performance on downstream tasks requiring localization abilities, mirroring the trend of image-level supervised pretrainings [14, 72].

Here, we propose a preliminary scaling study by pretraining on ImageNet-21k dataset with LOCA with a Base and a Large models. Results are shown in Fig. 6. Consistent with previous works on scaling image-level supervised ViTs [72], we observe that we need to scale both datasets and model capacity to achieve the best of performance. Interestingly, we observe that pretraining our method on the full ImageNet-21k dataset gives better transfer performance on ADE20k than using the highly curated ImageNet-1k split only (see 47.9 vs 48.5 in Tab. 7). This is not the case for all self-supervised learning methods as recently observed by [36]. While these preliminary results give promising signal about LOCA scalability, we note that ImageNet-21k is a relatively curated dataset and we would still need to probe our model on large, *uncurated* data [9, 27, 36, 57].

5. Conclusion

In this work, we have studied localization as an alternative pretraining strategy for Vision Transformers. We have shown that it results in spatially-aware features that transfer competitively to several challenging semantic segmentation benchmarks. We believe a promising direction for future work is to combine localization objectives with global image-level ones [7, 74]. Finally, we have focused on semantic segmentation in this paper as it is representative of tasks requiring spatial reasoning. However, the set of visual task with localization is very large and we hope that our findings can serve as a useful checkpoint for future studies beyond the scope of semantic segmentation or even beyond the scope of still images.

Acknowledgement. We thank Anurag Arnab, Lucas Beyer, Mostafa Dehghani, Ahmet Iscen, Thomas Lucas, Matthias Minderer, Basil Mustafa, Xingyi Zhou as well as the entire Ganesha team and Grand Vision group for their precious help, support and discussions around this project.

References

- [1] Jean-Baptiste Alayrac, Jeff Donahue, Pauline Luc, Antoine Miech, Iain Barr, Yana Hasson, Karel Lenc, Arthur Mensch, Katie Millican, Malcolm Reynolds, et al. Flamingo: a visual language model for few-shot learning. *arXiv preprint arXiv:2204.14198*, 2022. [1](#)
- [2] Yuki Markus Asano, Christian Rupprecht, and Andrea Vedaldi. Self-labelling via simultaneous clustering and representation learning. In *ICLR*, 2020. [4](#)
- [3] Mahmoud Assran, Mathilde Caron, Ishan Misra, Piotr Bojanowski, Florian Bordes, Pascal Vincent, Armand Joulin, Mike Rabbat, and Nicolas Ballas. Masked siamese networks for label-efficient learning. In *ECCV*, 2022. [1](#), [2](#), [3](#), [4](#), [11](#)
- [4] Mahmoud Assran, Mathilde Caron, Ishan Misra, Piotr Bojanowski, Armand Joulin, Nicolas Ballas, and Michael Rabbat. Semi-supervised learning of visual features by non-parametrically predicting view assignments with support samples. In *ICCV*, 2021. [4](#)
- [5] Alexei Baevski, Wei-Ning Hsu, Qiantong Xu, Arun Babu, Jiatuo Gu, and Michael Auli. Data2vec: A general framework for self-supervised learning in speech, vision and language. *arXiv preprint arXiv:2202.03555*, 2022. [1](#), [12](#)
- [6] Hangbo Bao, Li Dong, and Furu Wei. Beit: Bert pre-training of image transformers. *arXiv preprint arXiv:2106.08254*, 2021. [1](#), [2](#)
- [7] Adrien Bardes, Jean Ponce, and Yann LeCun. Vicregl: Self-supervised learning of local visual features. In *NeurIPS*, 2021. [8](#)
- [8] Nicolas Carion, Francisco Massa, Gabriel Synnaeve, Nicolas Usunier, Alexander Kirillov, and Sergey Zagoruyko. End-to-end object detection with transformers. In *ECCV*, 2020. [2](#), [7](#)
- [9] Mathilde Caron, Piotr Bojanowski, Julien Mairal, and Armand Joulin. Unsupervised pre-training of image features on non-curated data. In *ICCV*, 2019. [8](#)
- [10] Mathilde Caron, Ishan Misra, Julien Mairal, Priya Goyal, Piotr Bojanowski, and Armand Joulin. Unsupervised learning of visual features by contrasting cluster assignments. In *NeurIPS*, 2020. [1](#), [2](#), [4](#), [7](#)
- [11] Mathilde Caron, Hugo Touvron, Ishan Misra, Hervé Jégou, Julien Mairal, Piotr Bojanowski, and Armand Joulin. Emerging properties in self-supervised vision transformers. In *ICCV*, 2021. [1](#), [2](#), [4](#), [6](#), [7](#), [12](#), [13](#)
- [12] Joao Carreira and Andrew Zisserman. Quo vadis, action recognition? a new model and the kinetics dataset. In *CVPR*, pages 6299–6308, 2017. [1](#)
- [13] Ting Chen, Simon Kornblith, Mohammad Norouzi, and Geoffrey Hinton. A simple framework for contrastive learning of visual representations. *preprint arXiv:2002.05709*, 2020. [1](#), [2](#), [4](#)
- [14] Xi Chen, Xiao Wang, Soravit Changpinyo, AJ Piergiovanni, Piotr Padlewski, Daniel Salz, Sebastian Goodman, Adam Grycner, Basil Mustafa, Lucas Beyer, et al. Pali: A jointly-scaled multilingual language-image model. *arXiv preprint arXiv:2209.06794*, 2022. [1](#), [8](#)
- [15] Xinlei Chen, Saining Xie, and Kaiming He. An empirical study of training self-supervised vision transformers. In *ICCV*, 2021. [2](#), [6](#), [7](#), [13](#)
- [16] Yubei Chen, Adrien Bardes, Zengyi Li, and Yann LeCun. Intra-instance vicreg: Bag of self-supervised image patch embedding. *arXiv preprint arXiv:2206.08954*, 2022. [1](#)
- [17] Yingyi Chen, Xi Shen, Yahui Liu, Qinghua Tao, and Johan AK Suykens. Jigsaw-vit: learning jigsaw puzzles in vision transformer. *arXiv preprint arXiv:2207.11971*, 2022. [2](#)
- [18] Jang Hyun Cho, Utkarsh Mall, Kavita Bala, and Bharath Hariharan. Picie: Unsupervised semantic segmentation using invariance and equivariance in clustering. In *CVPR*, 2021. [2](#)
- [19] Marius Cordts, Mohamed Omran, Sebastian Ramos, Timo Rehfeld, Markus Enzweiler, Rodrigo Benenson, Uwe Franke, Stefan Roth, and Bernt Schiele. The cityscapes dataset for semantic urban scene understanding. In *CVPR*, 2016. [4](#), [6](#), [7](#), [12](#)
- [20] Zhigang Dai, Bolun Cai, Yugeng Lin, and Junying Chen. Up-detr: Unsupervised pre-training for object detection with transformers. In *CVPR*, 2021. [2](#), [4](#), [7](#)
- [21] Mostafa Dehghani, Alexey Gritsenko, Anurag Arnab, Matthias Minderer, and Yi Tay. Scenic: A jax library for computer vision research and beyond. In *CVPR*, 2022. [4](#)
- [22] Carl Doersch, Abhinav Gupta, and Alexei A Efros. Unsupervised visual representation learning by context prediction. In *ICCV*, 2015. [2](#)
- [23] Alexey Dosovitskiy, Lucas Beyer, Alexander Kolesnikov, Dirk Weissenborn, Xiaohua Zhai, Thomas Unterthiner, Mostafa Dehghani, Matthias Minderer, Georg Heigold, Sylvain Gelly, et al. An image is worth 16x16 words: Transformers for image recognition at scale. *preprint arXiv:2010.11929*, 2020. [1](#), [3](#)
- [24] Alexey Dosovitskiy, Philipp Fischer, Jost Tobias Springenberg, Martin Riedmiller, and Thomas Brox. Discriminative unsupervised feature learning with exemplar convolutional neural networks. *TPAMI*, 2016. [2](#), [6](#)
- [25] Mark Everingham, Luc Van Gool, Christopher KI Williams, John Winn, and Andrew Zisserman. The pascal visual object classes (voc) challenge. *IJCV*, 2010. [4](#), [7](#), [12](#)
- [26] Spyros Gidaris, Praveer Singh, and Nikos Komodakis. Unsupervised representation learning by predicting image rotations. *arXiv preprint arXiv:1803.07728*, 2018. [6](#)
- [27] Priya Goyal, Mathilde Caron, Benjamin Lefaudeux, Min Xu, Pengchao Wang, Vivek Pai, Mannat Singh, Vitaliy Liptchinsky, Ishan Misra, Armand Joulin, and Piotr Bojanowski. Self-supervised pretraining of visual features in the wild. *arXiv preprint arXiv:2103.01988*, 2021. [8](#)
- [28] Priya Goyal, Dhruv Mahajan, Abhinav Gupta, and Ishan Misra. Scaling and benchmarking self-supervised visual representation learning. In *ICCV*, 2019. [2](#)
- [29] Jean-Bastien Grill, Florian Strub, Florent Altché, Corentin Tallec, Pierre H Richemond, Elena Buchatskaya, Carl Doersch, Bernardo Avila Pires, Zhaohan Daniel Guo, Mohammad Gheshlaghi Azar, Bilal Piot, Koray Kavukcuoglu, Rémi Munos, and Michal Valko. Bootstrap your own latent: A new approach to self-supervised learning. In *NeurIPS*, 2020. [1](#), [2](#), [7](#), [12](#)

- [30] Mark Hamilton, Zhoutong Zhang, Bharath Hariharan, Noah Snavely, and William T Freeman. Unsupervised semantic segmentation by distilling feature correspondences. In *ICLR*, 2022. 2
- [31] Kaiming He, Xinlei Chen, Saining Xie, Yanghao Li, Piotr Dollár, and Ross Girshick. Masked autoencoders are scalable vision learners. In *CVPR*, 2022. 1, 2, 6, 7, 12, 13
- [32] Kaiming He, Haoqi Fan, Yuxin Wu, Saining Xie, and Ross Girshick. Momentum contrast for unsupervised visual representation learning. In *CVPR*, 2020. 1, 2, 4
- [33] Kaiming He, Georgia Gkioxari, Piotr Dollár, and Ross Girshick. Mask r-cnn. In *ICCV*, 2017. 7
- [34] Hanzhe Hu, Fangyun Wei, Han Hu, Qiwei Ye, Jinshi Cui, and Liwei Wang. Semi-supervised semantic segmentation via adaptive equalization learning. *NeurIPS*, 2021. 8
- [35] Dahun Kim, Donghyeon Cho, Donggeun Yoo, and In So Kweon. Learning image representations by completing damaged jigsaw puzzles. In *WACV*, 2018. 2
- [36] Skanda Koppula, Yazhe Li, Evan Shelhamer, Andrew Jaegle, Nikhil Parthasarathy, Relja Arandjelovic, João Carreira, and Olivier Hénaff. Where should i spend my flops? efficiency evaluations of visual pre-training methods. *arXiv preprint arXiv:2209.15589*, 2022. 8
- [37] Hsin-Ying Lee, Jia-Bin Huang, Maneesh Singh, and Ming-Hsuan Yang. Unsupervised representation learning by sorting sequences. In *ICCV*, 2017. 2
- [38] Yanghao Li, Hanzi Mao, Ross Girshick, and Kaiming He. Exploring plain vision transformer backbones for object detection. *arXiv preprint arXiv:2203.16527*, 2022. 4, 13
- [39] Tsung-Yi Lin, Michael Maire, Serge Belongie, James Hays, Pietro Perona, Deva Ramanan, Piotr Dollár, and C Lawrence Zitnick. Microsoft coco: Common objects in context. In *ECCV*, 2014. 1, 13
- [40] Zhuang Liu, Hanzi Mao, Chao-Yuan Wu, Christoph Feichtenhofer, Trevor Darrell, and Saining Xie. A convnet for the 2020s. In *CVPR*, 2022. 7
- [41] Ilya Loshchilov and Frank Hutter. Fixing weight decay regularization in adam. 2018. 4, 12
- [42] Tomas Mikolov, Kai Chen, Greg Corrado, and Jeffrey Dean. Efficient estimation of word representations in vector space. *arXiv preprint arXiv:1301.3781*, 2013. 2
- [43] Matthias Minderer, Alexey Gritsenko, Austin Stone, Maxim Neumann, Dirk Weissenborn, Alexey Dosovitskiy, Aravindh Mahendran, Anurag Arnab, Mostafa Dehghani, Zhuoran Shen, et al. Simple open-vocabulary object detection with vision transformers. *arXiv preprint arXiv:2205.06230*, 2022. 1, 4
- [44] Roozbeh Mottaghi, Xianjie Chen, Xiaobai Liu, Nam-Gyu Cho, Seong-Whan Lee, Sanja Fidler, Raquel Urtasun, and Alan Yuille. The role of context for object detection and semantic segmentation in the wild. In *CVPR*, 2014. 4, 6, 7, 12
- [45] T Nathan Mundhenk, Daniel Ho, and Barry Y Chen. Improvements to context based self-supervised learning. In *CVPR*, 2018. 2
- [46] Mehdi Noroozi and Paolo Favaro. Unsupervised learning of visual representations by solving jigsaw puzzles. In *ECCV*, 2016. 2
- [47] Deepak Pathak, Philipp Krahenbuhl, Jeff Donahue, Trevor Darrell, and Alexei A Efros. Context encoders: Feature learning by inpainting. In *CVPR*, 2016. 2
- [48] Pedro O Pinheiro, Amjad Almahairi, Ryan Y Benmaleck, Florian Golemo, and Aaron Courville. Unsupervised learning of dense visual representations. 2020. 2
- [49] Alec Radford, Jong Wook Kim, Chris Hallacy, Aditya Ramesh, Gabriel Goh, Sandhini Agarwal, Girish Sastry, Amanda Askell, Pamela Mishkin, Jack Clark, et al. Learning transferable visual models from natural language supervision. 2021. 1
- [50] Byungseok Roh, Wuhyun Shin, Ildoo Kim, and Sungwoong Kim. Spatially consistent representation learning. In *CVPR*, 2021. 2
- [51] Olga Russakovsky, Jia Deng, Hao Su, Jonathan Krause, Sanjeev Satheesh, Sean Ma, Zhiheng Huang, Andrej Karpathy, Aditya Khosla, Michael Bernstein, Alexander C Berg, and Li Fei-Fei. Imagenet large scale visual recognition challenge. *IJCV*, 2015. 1, 4
- [52] Rodrigo Santa Cruz, Basura Fernando, Anoop Cherian, and Stephen Gould. Deeppermnet: Visual permutation learning. In *CVPR*, 2017. 2
- [53] Mert Bulent Sariyildiz, Yannis Kalantidis, Karteek Alahari, and Diane Larlus. Improving the generalization of supervised models. *arXiv:2206.15369*, 2022. 7
- [54] Oriane Siméoni, Gilles Puy, Huy V Vo, Simon Roburin, Spyros Gidaris, Andrei Bursuc, Patrick Pérez, Renaud Marlet, and Jean Ponce. Localizing objects with self-supervised transformers and no labels. *arXiv preprint arXiv:2109.14279*, 2021. 2
- [55] Andreas Steiner, Alexander Kolesnikov, Xiaohua Zhai, Ross Wightman, Jakob Uszkoreit, and Lucas Beyer. How to train your vit? data, augmentation, and regularization in vision transformers. *arXiv preprint arXiv:2106.10270*, 2021. 2, 6, 7, 12
- [56] Robin Strudel, Ricardo Garcia, Ivan Laptev, and Cordelia Schmid. Segmenter: Transformer for semantic segmentation. In *ICCV*, 2021. 4, 6, 7, 12
- [57] Yonglong Tian, Olivier J Henaff, and Aäron van den Oord. Divide and contrast: Self-supervised learning from uncurred data. In *ICCV*, 2021. 8
- [58] Hugo Touvron, Matthieu Cord, Matthijs Douze, Francisco Massa, Alexandre Sablayrolles, and Hervé Jégou. Training data-efficient image transformers & distillation through attention. *preprint arXiv:2012.12877*, 2020. 6, 7
- [59] Hugo Touvron, Matthieu Cord, and Hervé Jégou. Deit iii: Revenge of the vit. *arXiv preprint arXiv:2204.07118*, 2022. 2, 6, 7, 8, 12, 13
- [60] Wouter Van Gansbeke, Simon Vandenhende, Stamatios Georgoulis, and Luc Van Gool. Unsupervised semantic segmentation by contrasting object mask proposals. In *ICCV*, 2021. 2
- [61] Xinlong Wang, Rufeng Zhang, Chunhua Shen, Tao Kong, and Lei Li. Dense contrastive learning for self-supervised visual pre-training. In *CVPR*, 2021. 2
- [62] Chen Wei, Haoqi Fan, Saining Xie, Chao-Yuan Wu, Alan Yuille, and Christoph Feichtenhofer. Masked feature predic-

- tion for self-supervised visual pre-training. In *CVPR*, 2022. 2
- [63] Yixuan Wei, Han Hu, Zhenda Xie, Zheng Zhang, Yue Cao, Jianmin Bao, Dong Chen, and Baining Guo. Contrastive learning rivals masked image modeling in fine-tuning via feature distillation. *arXiv preprint arXiv:2205.14141*, 2022. 12
- [64] Philippe Weinzaepfel, Vincent Leroy, Thomas Lucas, Romain Brégier, Yohann Cabon, Vaibhav Arora, Leonid Antsfeld, Boris Chidlovskii, Gabriela Csurka, and Jérôme Revaud. Croco: Self-supervised pre-training for 3d vision tasks by cross-view completion. In *NeurIPS*, 2022. 1
- [65] Zhirong Wu, Yuanjun Xiong, Stella X Yu, and Dahua Lin. Unsupervised feature learning via non-parametric instance discrimination. In *CVPR*, 2018. 2, 6
- [66] Tete Xiao, Colorado J Reed, Xiaolong Wang, Kurt Keutzer, and Trevor Darrell. Region similarity representation learning. In *ICCV*, 2021. 2
- [67] Zhenda Xie, Yutong Lin, Zheng Zhang, Yue Cao, Stephen Lin, and Han Hu. Propagate yourself: Exploring pixel-level consistency for unsupervised visual representation learning. In *CVPR*, 2021. 2
- [68] Zhenda Xie, Zheng Zhang, Yue Cao, Yutong Lin, Jianmin Bao, Zhuliang Yao, Qi Dai, and Han Hu. Simmim: A simple framework for masked image modeling. In *CVPR*, 2022. 1, 12
- [69] Jiahui Yu, Zirui Wang, Vijay Vasudevan, Legg Yeung, Mojtaba Seyedhosseini, and Yonghui Wu. Coca: Contrastive captioners are image-text foundation models. *arXiv preprint arXiv:2205.01917*, 2022. 1
- [70] Lu Yuan, Dongdong Chen, Yi-Ling Chen, Noel Codella, Xiyang Dai, Jianfeng Gao, Houdong Hu, Xuedong Huang, Boxin Li, Chunyuan Li, et al. Florence: A new foundation model for computer vision. *arXiv preprint arXiv:2111.11432*, 2021. 1
- [71] Shuangfei Zhai, Navdeep Jaitly, Jason Ramapuram, Dan Busbridge, Tatiana Likhomanenko, Joseph Yitan Cheng, Walter Talbott, Chen Huang, Hanlin Goh, and Joshua Susskind. Position prediction as an effective pretraining strategy. 2022. 1, 2, 4, 5
- [72] Xiaohua Zhai, Alexander Kolesnikov, Neil Houlsby, and Lucas Beyer. Scaling vision transformers. In *CVPR, year=2022*. 1, 8
- [73] Bolei Zhou, Hang Zhao, Xavier Puig, Sanja Fidler, Adela Barriuso, and Antonio Torralba. Scene parsing through ade20k dataset. In *CVPR*, 2017. 1, 4, 6, 7, 12
- [74] Jinghao Zhou, Chen Wei, Huiyu Wang, Wei Shen, Cihang Xie, Alan Yuille, and Tao Kong. ibot: Image bert pre-training with online tokenizer. *arXiv preprint arXiv:2111.07832*, 2021. 2, 6, 7, 8, 12, 13
- [75] Xingyi Zhou, Dequan Wang, and Philipp Krähenbühl. Objects as points. *arXiv preprint arXiv:1904.07850*, 2019. 13
- [76] Adrian Ziegler and Yuki M Asano. Self-supervised learning of object parts for semantic segmentation. In *CVPR*, 2022. 1, 2

Appendix

A. Pretraining with LOCA

A.1 Details on the patch feature prediction loss

In this section, we provide more details on the patch feature prediction loss. It can be seen as a “patch version” of the self-supervised loss used in the MSN framework [3]. Specifically, as mentioned in Section 3, we note $\mathbf{Z}_q \in \mathbb{R}^{d \times N_q}$ (resp. $\mathbf{Z}_{ref} \in \mathbb{R}^{d \times N_{ref}}$), the output patch representation matrix of the query (resp. reference) view. We project the output patch representations with a 2-layer multilayer perceptron (MLP) projection head, resulting in features $\tilde{\mathbf{Z}}_q \in \mathbb{R}^{\tilde{d} \times N_q}$ (resp. $\tilde{\mathbf{Z}}_{ref} \in \mathbb{R}^{\tilde{d} \times N_{ref}}$) with $\tilde{d} = 256$ in our experiments. We note $\mathbf{Q} \in \mathbb{R}^{\tilde{d} \times K}$ a set of K learnable prototypes, each of dimension \tilde{d} . In practice we use $K = 4096$. We compute a distribution based on the similarity between these prototypes and each patch output representation. Specifically, the prediction of the j^{th} patch feature in the query $\tilde{\mathbf{Z}}_q^j$ can be written:

$$\mathbf{p}_q^j = \text{softmax}(\tilde{\mathbf{Z}}_q^j \cdot \mathbf{Q} / \tau_q)$$

where τ_q is a temperature parameter set to 0.1 and both $\tilde{\mathbf{Z}}_q^j$ and \mathbf{Q} are L2-normalized. The goal of the network is to predict similar distributions for patches in the same location in the query and reference views. More precisely, the target distribution for prediction \mathbf{p}_q^j is that of the projected corresponding patch representation of the reference view:

$$\mathbf{p}_{ref}^i = \text{softmax}(\tilde{\mathbf{Z}}_{ref}^i \cdot \mathbf{Q} / \tau_{ref})$$

with $i = \mathbf{h}(j)$ and $\tau_{ref} < \tau_q$ (in practice we use $\tau_{ref} = 0.05$). Overall, the patch feature prediction objective that we minimize is:

$$\frac{1}{|\Omega|} \sum_{j \in \Omega} H(\mathbf{p}_{ref}^{\mathbf{h}(j)}, \mathbf{p}_q^j)$$

where H is the cross-entropy function and Ω is the set of patch position in the query that has an intersection with the reference (i.e. where \mathbf{h} is defined). The parameters of the branch processing the query views are updated by minibatch gradient descent. The parameters of the branch processing the reference views are updated via an exponential moving average of the encoder parameters processing the query views. We regularize this loss function with the mean entropy maximization (me-max) protocol [3]. More precisely in order to encourage the network to use the full set of prototypes \mathbf{Q} we maximize the entropy of the average prediction over all the patches of all the query views in a minibatch.

A.2 Implementation Details

We train our models with a base learning rate of 0.001 (linearly ramped up during the first 15 epochs before cosine

decay), a batch size of 1024 and a weight decay of 0.1 with adamw optimizer [41]. Models for ablations and analyses (in Sec. 4.1 and 4.3) are trained during 100 epochs while checkpoints in Sec. 4.2 and 4.4 are trained for 600 epochs. We use $\eta = 0.8$ for masking. For data augmentation we apply random resized crop, horizontal flipping and color jittering (following the parameters from BYOL [29]). Momentum parameter is set to 0.996 and increased with a cosine schedule to 1 during training [11, 29, 74]. We typically use 10 queries per reference view. Results are reported with the weights from the momentum branch [11, 74].

B. Transfer to Semantic Segmentation

B.1 Datasets

ADE20K [73]. It is a dataset containing scenes with fine-grained labels with 150 semantic classes and is one of the most challenging semantic segmentation datasets. The training split is composed of 20,210 images. We report results on the validation set, composed of 2,000 images.

Pascal Context [44]. The training split is composed of 4,998 images with 59 semantic classes and a background class (hence a total of 60 classes). The validation set has 5,105 images.

Pascal VOC [25]. This dataset has a training set of 10,582 images and counts 21 classes (with background class). We report results on the validation set, it has 1,449 images.

Cityscapes [19]. The dataset contains 5,000 images from 50 different cities. We consider the setup with 19 classes. There are 2,975 images in the training set, 500 images in the validation set and 1,525 images in the test set (which we do not use). We report results on the validation set.

B.2 Evaluation protocol

We precisely follow the experimental setup of Segmenter [56] for end-to-end finetuning of Vision Transformer with linear decoder. For data augmentation during training we apply normalization, random resizing of the image to a ratio between 0.5 and 2.0, photometric jittering and random horizontal flipping. We randomly crop images and use padding to preserve aspect ratio. We use the 512×512 resolution for ADE20k, Pascal VOC and Pascal Context and 768×768 on Cityscapes. On ADE20k, we train for 127 epochs with minibatch size of 16 (resulting in 160k iterations). On Pascal, we train for 256 epochs with minibatch size of 16 (resulting in 80k iterations). On Cityscapes, we train for 215 epochs with minibatch size of 8 (resulting in 80k iterations). We use the ‘‘poly’’ learning rate decay schedule and sweep the base learning rate in

Table 6. **Comparison to previous results with UperNet.** We report mean IoU for semantic segmentation on the validation set of ADE20k for different self-supervised and supervised representation learning methods. All models use the popular ViT-Base/16 architecture and are pre-trained on ImageNet-1k before being end-to-end finetuned on ADE20k. Results are reported in single-scale mode.

Method	ADE20k
<i>Supervised on ImageNet-1k</i>	
Supervised used in MAE [31]	47.4
DeiT-III [59]	49.3
<i>Self-supervised on ImageNet-1k without labels</i>	
DINO [11]	47.2
SimMIM [68]	47.6
FD-DINO [63]	47.7
MAE [31]	48.1
data2vec [5]	48.2
iBOT [74]	48.4
LOCA (Ours)	<u>48.5</u>

Table 7. **Scaling behavior on ImageNet-21k.** We report performance (mean IoU on ADE20k - single scale evaluation) for different pretrained LOCA models. ‘‘Rand- x ’’ means that we take a random subset of size x in ImageNet-21k. ‘‘INet-1k’’ means that we use the ImageNet-1k dataset only for pretraining.

Method / Split	Rand-130k	Rand-1.3M	Full 13M	INet-1k
ViT-Base	41.4	46.9	48.5	47.9
ViT-Large	39.1	48.5	52.5	-

$\{1e - 4, 3e - 4, 8e - 4\}$ for all of our runs. Weight-decay is kept fixed at 0.01. At evaluation time, we use the sliding-window mechanism with window resolution matching the resolution used during training (i.e. 512×512 for Pascal and ADE20k and 768×768 for Cityscapes) to handle varying image sizes during inference. Table 3 row 6 in [56] reports 48.06 mIoU (single scale) for finetuning from ViT-B/16 AugReg checkpoint [55]. Average of 6 runs in the same setup in our codebase gives 47.6 ± 0.4 mIoU.

C. Additional Results

UperNet decoder. In the main paper, we report results for semantic segmentation with end-to-end finetuning using the linear decoder from Segmenter [56]. In Table 6, we propose to compare to previously published results with the UperNet decoder [56]. Note that UperNet is a much more complex decoder than linear with 5300 times more parameters (76.8M parameters for UperNet versus only 14k for linear). As a matter of fact, UperNet decoder alone is composed of almost the same number of parameters than the ViT-Base backbone. Therefore, adapting a ViT-Base to semantic segmentation with UperNet results in doubling the total param-

Table 8. **Object detection with ViTDet.** We report Average Precision for object detection with CenterNet [75] and ViTDet adaptation protocol [38] on COCO dataset [39]. We follow the standard training schedule of 100 epochs. Architecture is ViT-B for all runs and pretraining data is ImageNet-1k.

Method	AP	AP50	AP75
DINO [11]	48.5	68.9	52.8
MoCo-v3 [15]	48.8	69.4	53.0
Supervised - DeiT-III [59]	49.0	69.5	53.4
LOCA (Ours)	49.6	70.0	54.1
iBOT [74]	49.9	70.6	54.3
MAE [31]	52.5	71.9	57.5

eter count of the model and training from scratch half of these parameters. Note that the reported 48.4mIoU performance for iBOT in Table 6 differs from the reported number in the iBOT paper [74] because recent correspondence with the authors has let us know that 50.0 is the best of 5 runs while 48.4 is the average. Following previous works, we use the 160,000 steps schedule (i.e. we use a minibatch size of 16 and train during 127 epochs). We observe in Table 6 that LOCA still performs competitively when evaluating in this setting.

Scaling behavior. We report in Table 7 the corresponding numbers for Figure 6 of the main paper.

Object detection with ViTDet. Finally, we propose to evaluate LOCA features when transferring to object detection. We consider the COCO dataset [39] and use the CenterNet detector [75] on a ViTDet backbone [38]. We observe in Table 8 that LOCA is competitive on this benchmark with other strong representation learning methods such as supervised DeiT-III [59] or iBOT [74]. Remarkably, MAE features are excellent on this benchmark and outperform all other backbones by a significant margin. Note that ViTDet protocol has been developed for MAE features and it is interesting to see that it does not seem to transfer well to other pretrained weights. We leave further investigation on transfer to object detection for future work.

D. Visualizations

In this section, we visualize the output of the pretraining task. Specifically, in Figure 7, we visualize query location prediction for different LOCA models. We compare models pretrained with different masking rates: (i) $\eta = 0$: no masking, the reference is entirely visible to the query; (ii) $\eta = 0.8$: default masking rate, only 40 reference patch tokens are visible to the query; (iii) $\eta = 1$: full masking, the reference is invisible to the query.

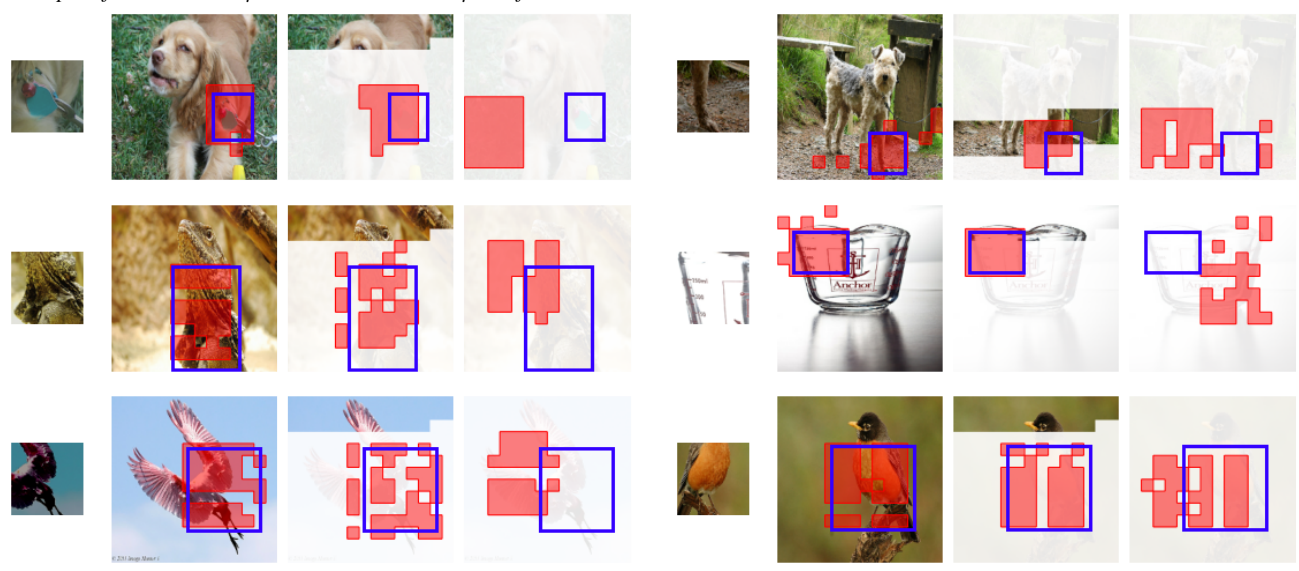
In the first rows of Figure 7, we show examples where

the network seems to effectively solve the task by *relative location*. In those cases, we observe that LOCA trained with masking rate $\eta = 0.8$ manages to locate the query based on the patches visible from the reference. For example we see that the network successfully manages to locate the leash joint based on seeing the patch representations of the head of the dog, or to locate the neck of the lizard based on the visible patches of its head. By contrast, the network which does not see the reference at all (i.e. $\eta = 1$) cannot successfully locate the query in those cases. Interestingly, we see that in some cases, this network ($\eta = 1$) can still locate the query by learning where things are typically located in natural images. For example, we observe in Figure 7 that by recognizing a part such as “ear” it makes a guess that it is more likely to be at the top of the image rather than at the bottom. However, it cannot guess if it is left or right because we apply random horizontal flips between query and reference during training and so this patch is as likely to occur at the right than at the left of the image.

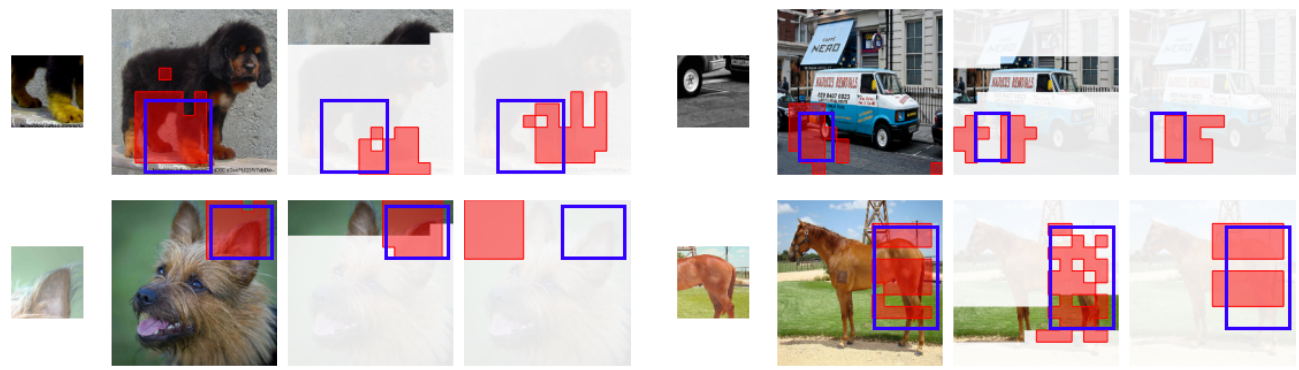
Lastly, we observe that the network trained with full access to the reference ($\eta = 0$) can almost always locate the query. This is because it can rely on low-level cues such as edge consistency or salient points. The last rows of Figure 7 illustrate this phenomenon.

query $\eta = 0$ $\eta = 0.8$ $\eta = 1$ query $\eta = 0$ $\eta = 0.8$ $\eta = 1$

Example of cases where $\eta = 0.8$ succeeds and $\eta = 1$ fails. The network relies on relative location.



Example of cases where the query location can easily be inferred from looking at query alone.



Example of cases where the network relies on low-level cues. Only the variant with $\eta = 0$ succeeds.

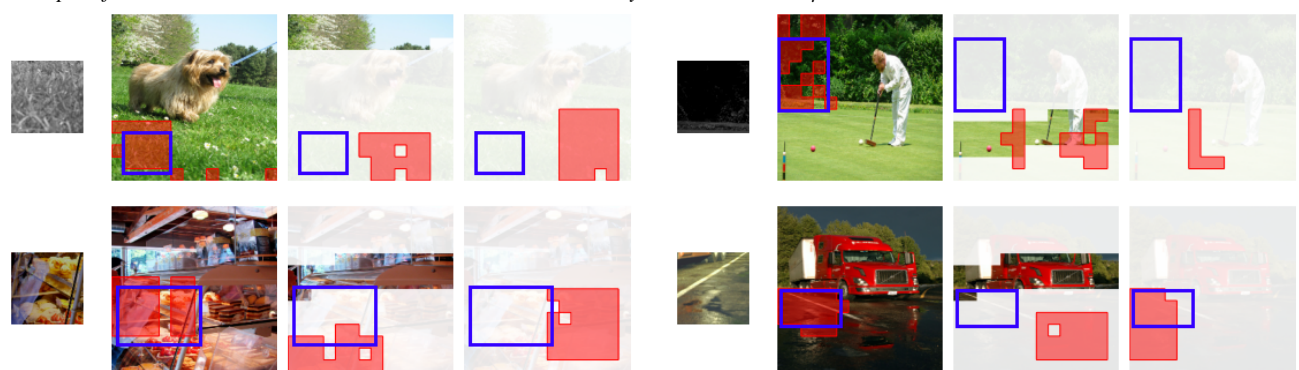


Figure 7. **Visualizing LOCA’s predictions.** The query location is shown in blue in the reference and LOCA predictions are shown in red. Columns correspond to different reference masking rates and we show only patches visible to the query when it makes its prediction. Displayed images are not seen during training. See discussion in Section D.